Spectroscopic and DFT Study of Tungstic Acid Peroxocomplexes

Laura Barrio, José M. Campos-Martín, and José L. G. Fierro*

Instituto de Catálisis y Petroleoquímica, CSIC, Marie Curie, 2, Cantoblanco, 28049 Madrid, Spain

Received: October 20, 2006; In Final Form: January 9, 2007

The catalytic system formed by tungstic acid and its complexes with H_2O_2 and phenylphosphonic acid has been analyzed from the experimental and theoretical points of view. Previous structural studies by XRD proved the validity of the DFT proposed models and methodology. Hydrogen peroxide reacts with tungstic acid to form a peroxo complex. Vibrational and electronic spectra showed significant changes upon interaction with H_2O_2. The DFT and TD-DFT for IR and UV−vis calculations not only are in agreement with experimental data but also allow for a deeper characterization of the species formed in in situ conditions. A SCRF/PCM methodology was chosen to account for the solvent effect. The solvent effect of water was considered for geometry re-optimization of the structure and for the TD-DFT calculations.

Introduction

Oxidation reactions are a fundamental part of the chemical industry and, more specifically, that portion related to converting petroleum based materials into useful chemicals. Molecular oxygen is the ideal oxidant, abundant and non-contaminating, but its reactivity is difficult to control. Hydrogen peroxide seems to be an attractive alternative for liquid phase oxidations because the only byproduct is water. Because of their catalytic activity and specialized redox behavior, tungstates have received special attention in a variety of industrial, pharmaceutical, and biological processes as they can be regarded as an environmentally friendly alternative to traditional oxidation reactions that represents an improvement in terms of pollution prevention.[1]

One the most attractive catalytic systems for H_2O_2 as an oxidant is tungstic acid, a phosphorus based acid as a cocatalyst and a quaternary ammonium salt as the phase transfer agent.[2] These catalysts are very attractive because tungstate catalysts are physiologically harmless, do not cause unproductive H_2O_2 decomposition, and can be applied to a wide variety of oxidation reactions.[1−6] A tungstic acid catalyst is useful with organic substrates such as alcohols or aldehydes, but the addition of phosphonic acid derivates is crucial for catalytic activity toward olefinic or sulfide and sulfoxide substrates.[2]

Hydrogen peroxide is commercially available as an aqueous solution. This fact implies the presence of two phases in the reaction system, at least for most of the organic subtrates. Because of this limitation, the best catalytic system of tungstic acid consists of phase transfer catalysts (PTC). The bibliography of ref 2 provides reliable data for the generally accepted mechanism for this reaction with a PTC, as depicted in Scheme 1, and describes experimental findings in the oxidation of organic substrates with hydrogen peroxide using tungsten catalysts. In the aqueous phase, the catalyst precursor $(HO)_2WO_2$ is rapidly oxidized by H_2O_2 to a bisperoxotungstate compound, which then reacts with phosphonic acid to form **1**. This anion moiety can easily be transferred to the organic phase by $H^+ - Q^+$ ion exchange to form **2**. Then, **2** oxidizes the organic substrate and forms an oxidized product **3**. The monoperoxo tungstate ion in **3** is reoxidized by H_2O_2 after returning to the aqueous phase as the ion pair **4**. This step may also occur at the organic−aqueous interface or even in the organic phase to some extent.

Because of the high industrial interest in such processes, it is of paramount importance to identify the species present in the reaction media and link them with the catalytic activity. To better understand these catalytic processes, a more detailed characterization of peroxotungstates is necessary. Computational chemistry, combined with other characterization techniques, is a key instrument for the identification of reaction species.

In light of the previous discussion, the present work was undertaken with the aim of studying the interactions between tungstic acid and hydrogen peroxide as a previous step to understand the oxidation reaction mechanism. We studied several chemical species involved in the oxidation reactions, combining the experimental data from infrared (FT-IR) and ultraviolet−visible (UV−vis) spectroscopy and the theoretical calculations using the density functional theory (DFT) approach. This combination of experimental and theoretical data was used in the assignment of the IR and UV−vis bands. The information found in this work will be helpful for identifying and analyzing the properties of the species present in reaction conditions. These species, which are quite difficult to find outside the reaction environment, are responsible for the catalytic activity in oxidation reactions. Therefore, they will be the main focus of our study.

Experimental and Computational Methods

Tungstic acid ($(HO)_2WO_2$), phenylphosphonic acid ($PhP(O)(OH)_2$), and hydrogen peroxide (50% solution) were purchased from Sigma-Aldrich. All compounds were used without further purification.

Infrared spectra were recorded at room temperature on a Nicolet 510 FT-IR spectrophotometer provided with a KBr beamsplitter and a DTGS detector, using KBr wafers containing 1% of the sample. For each spectrum, 100 scans were accumulated at a spectral resolution of 4 cm^{-1}. UV−vis spectra of the water diluted samples (10^{-5} M) were recorded on a Varian Cary 5000 spectrophotometer.

* Corresponding author. E-mail: jlgfierro@icp.csic.es. Fax: +34 915854760.

10.1021/jp066901x CCC: $37.00
Published on Web 02/28/2007

SCHEME 1: Proposed Mechanism of Phase Transfer Oxidation of Organic Compounds with Hydrogen Peroxide and Tungstic Acid Catalysts

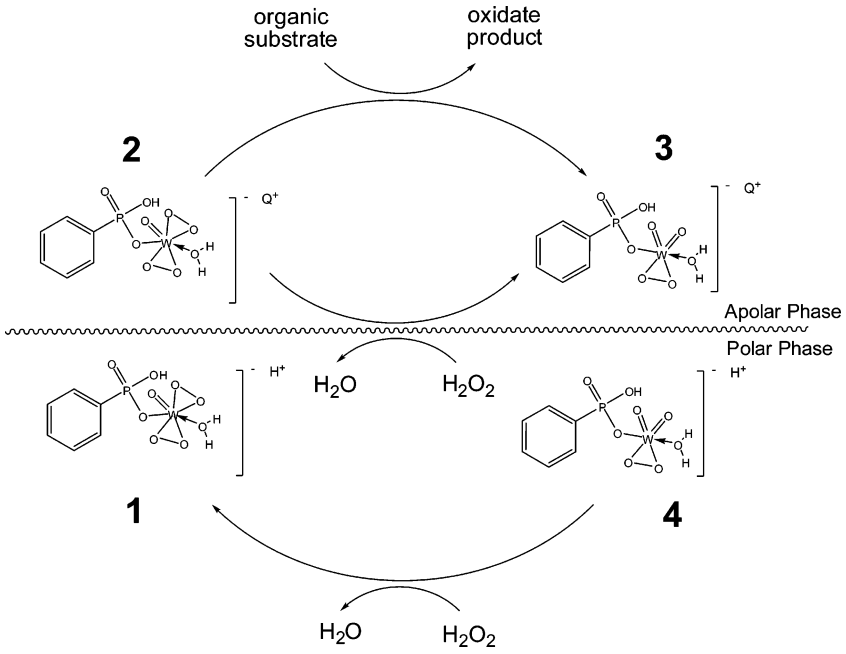

SCHEME 2: Structure of the Species Used in This Study

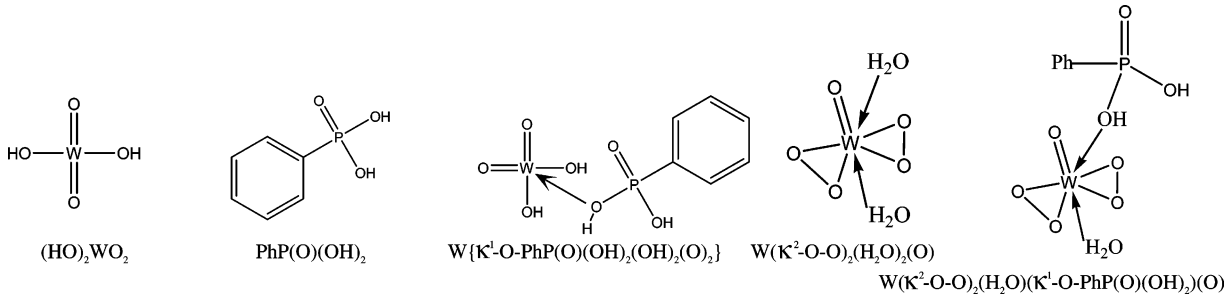

All calculations were performed with the Gaussian 03 program.[7] For W, a modified LANL2DZ basis set with a (541, 541, 211) contraction was employed.[8] This basis set includes additional functions of the 4p shell that are needed to account for charge transfer effects, which are so important in organometallic chemistry. For H, C, O, and P, a 6-311+G(3d,2p) basis set was chosen, in balance with the basis set employed for the metal. A full geometry optimization was carried out with the pure functional BPW91. DFT methodology was successfully tested for studying tungsten oxide clusters.[9] A BPW91 functional has been previously shown to be a reliable model for describing phosphoric tungsten complexes.[10] The frequency analysis performed revealed that all the structures were true minima. Scheme 2 shows the analyzed structures.

The solvent effect of water was also studied under the self-consistent reaction field approach by means of a polarizable continuum model (PCM), as implemented in Gaussian 03.[11] The PCM allows for a reliable description of the solvent effect by considering its dielectric constant and the solvent radius. To mimic the solute molecule's actual shape, the cavity was built as the envelope of a series of interlocking atomic spheres.[12] All the structures were fully re-optimized, taking into account the presence of water. A TD-DFT analysis with solvent effect was performed[12] with the B3PW91 functional. The solvent effect is included here at its full scale, not only by altering the geometry of the system but also by taking into account nonequilibrium solute−solvent effects during the light absorption process. The use of a hybrid functional was necessary for an accurate prediction of electronic transitions.[13] B3PW91 was chosen among hybrid functionals due to the good behavior of BPW91 for optimizing structures. Hybrid TD-DFT methodology was recently proven to reproduce the UV−vis spectra of polycyanotungsten complexes.[14]

Results and Discussion

In this study, the selected models are depicted in Scheme 2. These clusters represent, from starting compounds such tungstic acid ($(HO)_2WO_2$) or phenylphosphonic acid ($PhP(O)(OH)_2$), the complex formed between these two compounds ($W(\kappa^1$-O-PhP-$(O)(OH)_2(OH)_2(O)_2)$) and the corresponding biperoxo complexes ($W(\kappa^2$-O-$O)_2(H_2O)_2(O)$ and $W(\kappa^2$-O-$O)_2(H_2O)(\kappa^1$-O-PhP(O)-$(OH)_2)(O)$). These latter species are very important in the oxidation reaction mechanism because they are present in the reaction medium in the oxidations with hydrogen peroxide and are related to the reaction intermediates as described in the bibliography of ref 2 (Scheme 1).

It is well-known that tungsten peroxo complexes can easily dimerize. However, we have selected the monomeric peroxo species because it is the principal species in the presence of excess H_2O_2,[16,17] and an excess of hydrogen peroxide occurs when tungstic acid acts as a catalyst. For a better study of UV−vis spectra, this experiment was performed with a low concentration of compounds. In such dilute conditions, there is good

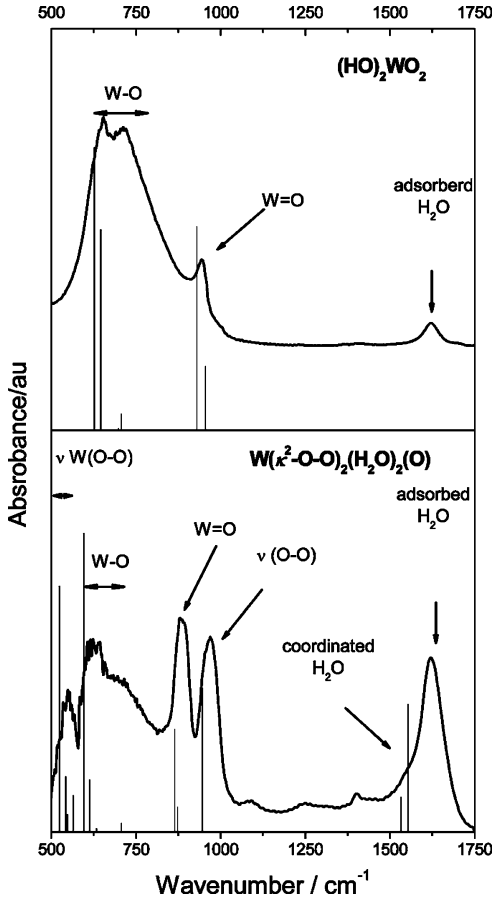

Figure 1. Experimental and theoretical IR spectra for tungstic acid and H_2O_2 treated samples.

TABLE 1: Selected Structural Data of $(HO)_2WO_2$ under C_2 Symmetry

bond distance (Å)	gas phase	water	experimental[18]
W═O	1.730	1.731	1.69
W−OH	1.909	1.914	1.93

TABLE 2: Selected Structural Data of $PhP(O)(OH)_2$

bond distance (Å)	gas phase	water	experimental[19]
P−OH	1.621	1.614	1.55
P═O	1.478	1.494	1.50
P−C	1.807	1.804	1.77

evidence for the rapid formation of the monomeric species with large formation constants. For instance, dimerization is not apparent at concentrations below 0.02 M.[17]

First of all, we will analyze the tungstic acid system. The main geometrical data obtained by our theoretical calculations are compiled in Table 1. The optimization process yielded a C_2 structure, very close to the one obtained experimentally by XRD.[18] The re-optimization step with solvent effects did not produce any significant changes in the structure. The theoretical model chosen along with the basis set employed seems to be appropriate due to the good agreement between experimental and theoretical structures.

The phenylphosphonic acid structure data are summarized in Table 2. The correlation with experimental XRD structure[19] is good, the major deviations being the P−OH bond distance. As was obtained by tungstic acid, the effect of solvent did not alter the geometry of the model.

A more interesting feature is the structure of the tungsten peroxo complex, which was obtained by the reaction of tungstic acid with H_2O_2 (see Table 3). The tungsten−peroxo bond distance determined by XRD[15] was well-reproduced by our model, and so was the metal−water molecule bond distance. This result implies that the inclusion of two water molecules in the model is consistent with the experimental observed structure.

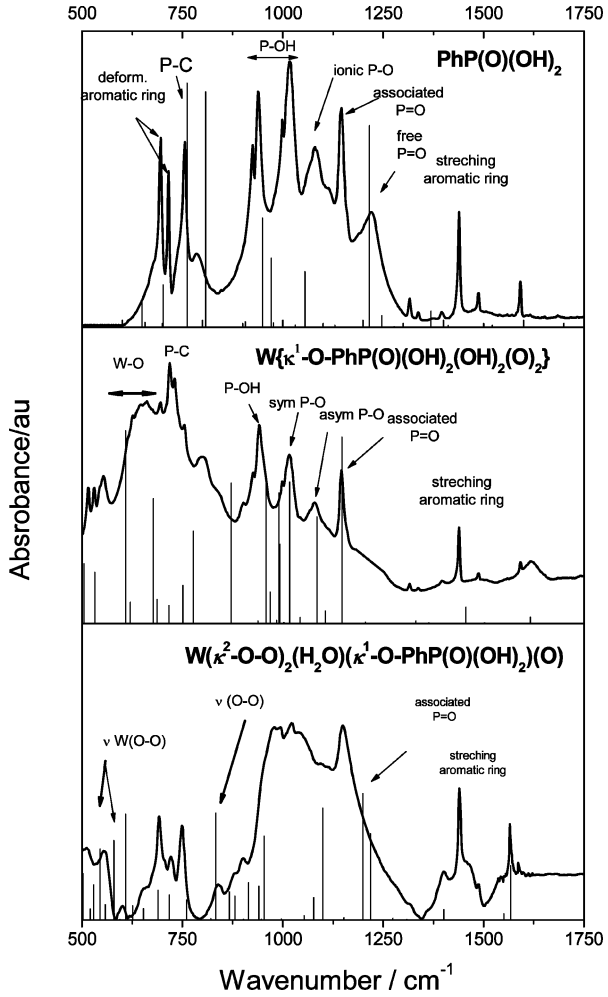

Figure 2. Experimental and theoretical IR spectra for phenylphosphonic acid, tungstic acid, and H_2O_2 treated samples.

TABLE 3: Selected Structural Data of $W(\kappa^2\text{-O-O})_2(H_2O)_2(O)$ Complex

bond distance (Å)	gas phase	water	experimental[15]
W−OH_2	2.346	2.374	2.30
W−OO	1.953	1.950	2.00
W═O	1.723	1.728	1.64

TABLE 4: Selected Structural Data of $W(\kappa^2\text{-O-O})_2(H_2O)(\kappa^1\text{-O-PhP(O)(OH)}_2)(O)$ Complex

bond distance (Å)	gas phase	water	experimental[20]
W−OH_2	2.487	2.402	
W−OO	1.962	1.969	1.97
W−O	1.717	1.729	1.62
P−C	1.784	1.778	
P═O	1.486	1.490	1.48
P−OH	1.759	1.724	

Finally, the structure of the tungsten−phosphoric peroxo complex is discussed. The experimental data[20] and theoretical results are summarized in Table 4. The metal−water molecule bond distance is elongated when compared to the tungsten−peroxo complex one, meaning that the interaction with water is weaker now. There is no reported experimental value to support such an effect. The tungsten−peroxo bond distance is

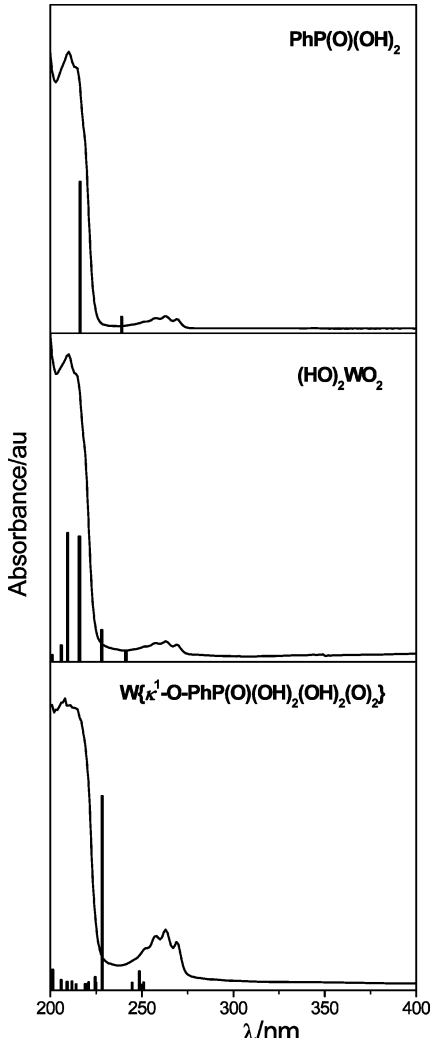

Figure 3. Experimental and theoretical UV−vis spectra of water diluted samples.

slightly reduced in the presence of phosphonic acid, and the agreement with experimental value is excellent. All the other relevant bond distances are quite similar to the previously analyzed compounds. When available, correlation with experimental XRD data is adequate.

Summing up the structural data for all the species considered, the geometrical results obtained by our models are in reasonable agreement with XRD data. This is a validation for the theoretical method and basis set employed. Moreover, it also confirms the validity of the structural models proposed from the complexes formed by the reaction of H_2O_2 with tungstic acid. Once the employment of our model was successfully tested by the structural results, it was time to analyze the spectroscopic behavior of the compounds.

The infrared spectrum of the $(HO)_2WO_2$ sample diluted in potassium bromide revealed the characteristic vibration bands of this compound (Figure 1). This spectrum shows a broad band at 600−700 cm^{-1} attributed to W−O···HO−W, W−O−H, and W−O−W bond vibrations[21,22] and a sharper band at 950 cm^{-1} assigned to W═O bond vibration.[21,22] The peak observed at 1620 cm^{-1} is due to the OH bending of molecular water absorbed in the KBr pellet. The spectrum of tungstic acid treated with hydrogen peroxide shows clear differences. The intensity of the bands attributed to the W−O and W−OH bond vibrations was clearly lower, and additional bands were observed. The ν(O−O) vibration appears as a clearly defined strong band at

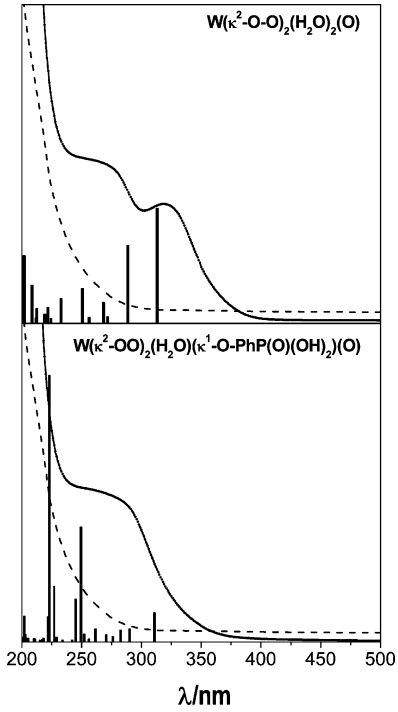

Figure 4. Experimental and theoretical UV−vis spectra of water diluted samples treated with hydrogen peroxide (dotted line, H_2O_2 solution).

around 870 cm^{-1}.[22] Additional bands in the range of 650−560 cm^{-1} belong to ν_{as}W(O−O) and ν_sW(O−O).[22] A weak shoulder at 1550 cm^{-1} can hardly be distinguished.

DFT calculations aimed at describing the vibrational structure of the two species point to good agreement with the experimental infrared spectra, as shown in Figure 1. The wavenumbers of the characteristic infrared bands described previously fit those predicted by the theoretical model fairly well. Additionally, the DFT calculations provide some interesting clues that initially could not be gained from inspection of the experimental infrared spectra. An example illustrating the potential of the DFT calculations is the prediction of a band at 1550 cm^{-1} attributed to the vibration of the OH bending of water molecules coordinated with the tungsten−biperoxocomplex that only appears as a shoulder in the experimental spectra because it was overshadowed by the vibration modes of H_2O adsorbed in the KBr pellet.

The phenylphosphonic acid infrared spectrum revealed the characteristic vibration bands of this compound (Figure 2). The most significant features are described subsequently: the peaks at 690, 720, and 1438 cm^{-1} correspond to the vibration of the aromatic ring,[23] and the peaks between 920 and 950 cm^{-1} and the peak at 1014 cm^{-1} are all assigned to P−OH bonds.[23−25] The bands at 1014 and 1075 cm^{-1} can be assigned to P−O stretching modes in the hydrogenophosphonate or phosphonate ions.[25] The bands at 1144 and 1212 cm^{-1} correspond to stretching vibrations of coordinated and free P═O bonds, respectively.[23,25] The DFT calculated spectrum is in good agreement with the experimental one and the assignments, except the peak at 1144 cm^{-1}, which cannot be predicted because these species are not considered in our model.

The infrared spectrum of the complex between tungstic acid and phenylphosphonic acid looks like the sum of individual spectra of both compounds; however careful study shows some differences (Figure 2). The peak of phenylphosphonic acid that appears at 1212 cm^{-1}, which corresponds to the free P═O bond vibration, is not present in the complex spectrum, although the

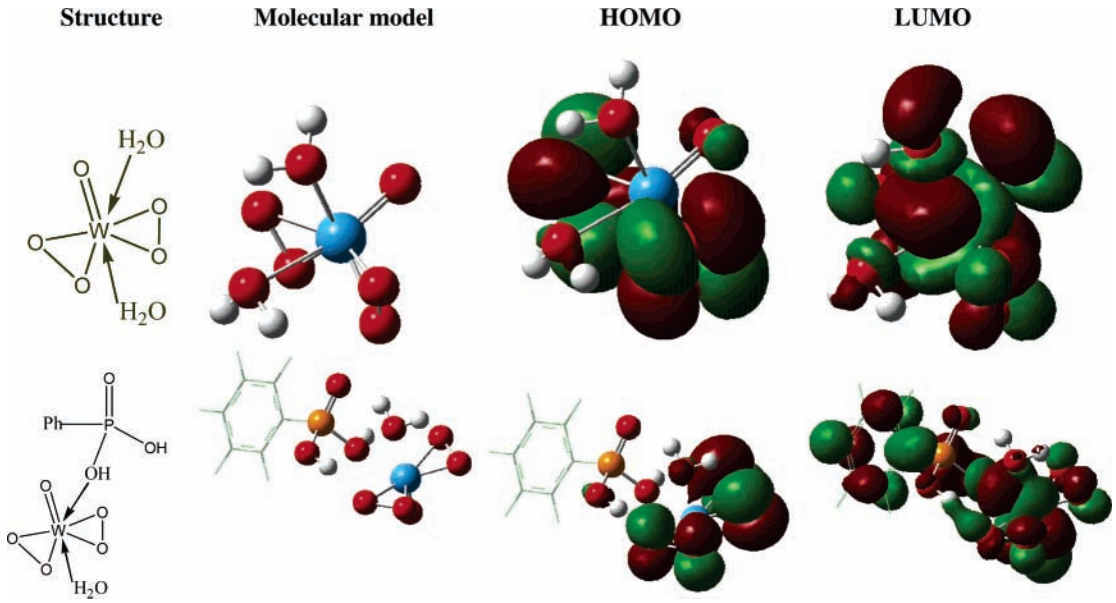

Figure 5. Molecular model and HOMO−LUMO involved in the less energetic electronic transition.

peak at 1144 cm^{-1} remains. This fact indicates an interaction between oxygen with tungstic acid. Two new peaks (532 and 512 cm^{-1}) are clearly present in the W(κ^1-O-PhP(O)$(OH)_2$$(OH)_2$-$(O)_2$) spectrum, which are not in the individual spectra. DFT results revealed that the vibrations in this region correspond to a flexion of the phenylphosphonic acid coupled with a tungstic acid one. The whole complex is involved simultaneously in these vibrational signals. IR spectrum of the complex calculated by DFT predicts the changes in the spectrum observed in the experimental one.

The spectrum of the complex between tungstic acid and phenylphosphonic acid treated with hydrogen peroxide showed some clear differences (Figure 2). The ν(O−O) vibration appears as a clear band at around 830 cm^{-1}.[22] Additional bands around 560 cm^{-1} belong to ν_{as}W(O−O) and ν_sW(O−O).[22] A series of peaks associated with phenylphosphonic acid are also present in addition to the band at 950 cm^{-1} assigned to the W═O vibration.[21,22]

DFT calculations aimed at describing the vibrational structure of the three species by way of a good agreement with the experimental infrared spectra (Figure 2). The main differences between experimental and theoretical vibration bands can be attributed to the interaction between clusters in the solid, which cannot be taken in the model employed in the calculations. However, the infrared spectra of the complex between tungstic acid and phenylphosphonic acid and its peroxo compound are clearly predicted with the DFT models.

UV−vis spectra of the samples dissolved in water are compared in Figure 3. The electronic spectra of $(HO)_2WO_2$ exhibited a band at 210 nm, which is characteristic of this compound. The spectrum of phenylphosphonic acid is quite similar with a band at 215 nm typical of the electronic spectrum of aromatic compounds. When both compounds are present in solution, a change in the spectrum is clearly observed: the band shifts to a lower wavelength as a consequence of the interaction between the two compounds. A weak band around 270 nm present in the three spectra could be attributed to the presence of an anionic/dissociated species of the acids. These experimental observations are satisfactorily described by theoretical calculations, and the shift to lower wavelengths observed in the catalyst and cocatalyst cluster spectra is clearly predicted. The weak band around 270 nm is not predicted because anionic/dissociated species of the acids are not taken into account by the model.

For the analysis of H_2O_2 treated samples, we employed an excess of hydrogen peroxide to ensure the presence of isolated biperoxotungten species.[22] A blank spectrum of hydrogen peroxide in water is shown for comparison purposes, although this spectrum did not interfere with the bands under study. These conditions simulate reaction conditions; when tungstic acid acts as catalyst, there is an excess of hydrogen peroxide with respect to $(HO)_2WO_2$. The H_2O_2 treated samples show different spectra (Figure 4). Two new bands at 265 and 325 nm are observed for the W(κ^2-O-O)$_2$(H_2O)$_2$(O) sample. These new bands are attributed to the presence of peroxo moieties and coordinated water molecules around the W center. But, the absorption band at 325 nm was absent when phenyl phosphonic acid was added. These observations and the differences observed between W(κ^2-O-O)$_2$(H_2O)$_2$(O) and W(κ^2-O-O)$_2$(H_2O)(κ^1-O-PhP(O)$(OH)_2$)(O) samples are consistently simulated by TD-DFT results.

Theoretical results allow not only the assignment of experimental absorption bands, but also to obtain a deeper knowledge of the nature of the transition involved in the absorption. This information can be gained by analyzing the molecular orbitals implied in the transition. The orbitals with the highest participation in the less energetic transition are depicted in Figure 5. For the W(κ^2-O-O)$_2$(H_2O)$_2$(O) complex, there is a HOMO−LUMO electron jump, in which the peroxo oxygens donate their electronic density to the tungsten atom during the transition. Thus, the observed electronic transition is due to an absorption in which the peroxo groups are involved. The peroxo moieties are needed to obtain the UV−vis spectra. Therefore, not only the experimental shift of the absorption band supports the existence of the peroxo complex but also the theoretical results are a good indicator of its presence.

A similar behavior was obtained for the W(κ^2-O-O)$_2$(H_2O)-(κ^1-O-PhP(O)$(OH)_2$)(O) complex. The first transition corresponds to a HOMO−LUMO jump, where the electronic density from the peroxo oxygens was transferred to the whole molecule. The π electronic cloud was received by the neighboring W atom but also by the distant aromatic structure from the phenylphosphonic acid. The probability, and hence the intensity, of an electronic transition is proportional to the overlap between the

initial and the final state. For the tungsten phosphonic peroxo complex, when the electron jumps from the HOMO to the LUMO, there is a severe reallocation of electronic density as can be seen in Figure 5. The overlap between the HOMO−LUMO orbitals is very small, and therefore, a much weaker transition is predicted by TD-DFT calculations. The nature of the first transition was not altered by the presence of phenylphosphonic acid, but its intensity decreased considerably. The whole molecule participates in this transition, and the experimental and theoretical results are needed to assign the involved species.

Conclusion

The good correlation found between experiment and theory underlines the importance of studying this catalytic system from both experimental and theoretical points of view. The structures obtained by DFT calculations are in full agreement with experimental XRD data. The validation of the proposed model by the structural characterization allows trustworthy analysis of theoretical spectroscopic data. Hydrogen peroxide reacts with tungstic acid to form a peroxo complex, which can be characterized experimentally by UV−vis and IR spectroscopy. The presence of coordinated water, as considered in the molecular model proposed, is corroborated by the experimental spectra. DFT calculations are able to reproduce the experimental UV−vis and IR spectra. They can also provide additional information about the structure of the observed complexes.

Acknowledgment. CTI (CSIC) and CESGA are acknowledged for providing CPU time. L.B. gratefully acknowledges a fellowship granted by Repsol-YPF (Spain).

Supporting Information Available: Cartesian coordinates for all optimized structures in the gas phase and the basis set input for the W atom. This material is available free of charge via the Internet at http://pubs.acs.org.

References and Notes

(1) Sato, K.; Aoki, M.; Noyori, R. *Science* **1998**, *281*, 1646.
(2) Noyori, R.; Aoki, M.; Sato, K. *Chem. Commun.* **2003**, 1977.
(3) De Vos, D. E.; Sels, B. F.; Jacobs, P. A. *Adv. Synth. Catal.* **2003**, *345*, 457.
(4) Lane, B. S.; Burgess, K. *Chem. Rev.* **2003**, *103*, 2457.
(5) Campos-Martín, J. M.; Capel-Sanchez, M. C.; Fierro, J. L. G. *Green Chem.* **2004**, *6*, 557.
(6) Karimi, B.; Ghoreishi-Nezhad, M.; Clark, J. H. *Org. Lett.* **2005**, *7*, 625.
(7) Frisch, M. J.; Trucks, G. W.; Schlegel, H. B.; Scuseria, G. E.; Robb, M. A.; Cheeseman, J. R.; Montgomery, J. A., Jr.; Vreven, T.; Kudin, K. N.; Burant, J. C.; Millam, J. M.; Iyengar, S. S.; Tomasi, J.; Barone, V.; Mennucci, B.; Cossi, M.; Scalmani, G.; Rega, N.; Petersson, G. A.; Nakatsuji, H.; Hada, M.; Ehara, M.; Toyota, K.; Fukuda, R.; Hasegawa, J.; Ishida, M.; Nakajima, T.; Honda, Y.; Kitao, O.; Nakai, H.; Klene, M.; Li, X.; Knox, J. E.; Hratchian, H. P.; Cross, J. B.; Bakken, V.; Adamo, C.; Jaramillo, J.; Gomperts, R.; Stratmann, R. E.; Yazyev, O.; Austin, A. J.; Cammi, R.; Pomelli, C.; Ochterski, J. W.; Ayala, P. Y.; Morokuma, K.; Voth, G. A.; Salvador, P.; Dannenberg, J. J.; Zakrzewski, V. G.; Dapprich, S.; Daniels, A. D.; Strain, M. C.; Farkas, O.; Malick, D. K.; Rabuck, A. D.; Raghavachari, K.; Foresman, J. B.; Ortiz, J. V.; Cui, Q.; Baboul, A. G.; Clifford, S.; Cioslowski, J.; Stefanov, B. B.; Liu, G.; Liashenko, A.; Piskorz, P.; Komaromi, I.; Martin, R. L.; Fox, D. J.; Keith, T.; Al-Laham, M. A.; Peng, C. Y.; Nanayakkara, A.; Challacombe, M.; Gill, P. M. W.; Johnson, B.; Chen, W.; Wong, M. W.; Gonzalez, C.; Pople, J. A. *Gaussian 03*, revision C.01; Gaussian, Inc.: Wallingford, CT, 2004.
(8) Couty, M; Hall, M. B. *J. Comput. Chem.* **1996**, *17*, 1359.
(9) Tsipsis, A. C.; Tsipis, C. A. *J. Phys. Chem. A* **2000**, *104*, 859.
(10) Rio, D.; Schubert, G.; Papai, I.; Galindo, A. *J. Organomet. Chem.* **2002**, *663*, 83.
(11) Cossi, M.; Scalmani, G.; Rega, N.; Barone, V. *J. Chem. Phys.* **2002**, *117*, 43.
(12) Cossi, M.; Barone, V. *J. Chem. Phys.* **2001**, *115*, 4708.
(13) Liao, M. S.; Lu, Y.; Scheiner, S. *J. Comput. Chem.* **2003**, *24*, 623.
(14) Barone, V.; Biani, F. F.; Ruiz, E.; Sieklucka, B. *J. Am. Chem. Soc.* **2001**, *123*, 10742.
(15) Pecquenard, B.; Castro-Garcia, S.; Livage, J.; Zavalij, P. Y.; Whittingham, M. S.; Thouvenot, R. *Chem. Mater.* **1998**, *10*, 1882.
(16) Stomberg, R. J. *Less-Common Met.* **1988**, *143*, 363.
(17) Dickman, M. H.; Pope, M. T. *Chem. Rev.* **1994**, *94*, 569.
(18) Szymansky, J. T.; Roberts A. C. *Can. Mineral.* **1984**, *22*, 681.
(19) Weakley, T. J. R. *Acta Crystallogr, Sect. B* **1976**, *32*, 2889.
(20) Salles, L.; Aubry, C.; Thouvenot, R.; Roberte, F.; Doremiexu-Morin, C.; Chottard, G.; Ledon, H.; Jeannin, Y.; Bregeault, J. M. *Inorg. Chem.* **1994**, *33*, 871.
(21) Nakamoto, K. In *Infrared and Raman Spectra of Inorganic and Coordination Compounds*, 5th ed.; John Wiley and Sons Inc.: New York, 1997; Part B.
(22) Hou, S. Y.; Zhou, Z. H.; Lin, T. R.; Wan, H. L. *Eur. J. Inorg. Chem.* **2006**, 1670.
(23) Thomas, C.; Chittenden, R. A. *Spectrochim. Acta* **1964**, *20*, 467.
(24) Botelho do Rego, A. M.; Ferraria, A. M.; El Beghdadi, J.; Debontridder, F.; Brogueira, P.; Naaman, R.; Rei Vilar, M. *Langmuir* **2005**, *21*, 8765.
(25) Ohno, K.; Mandai, Y.; Matsuura, H. *J. Mol. Struct.* **1993**, *298*, 1.